03,07,09

NV$^-$ defects in silicon carbide for quantum magnetometry

© S.S. Nagalyuk[1], O.P. Kazarova[1], P.A. Kosach[2], E.N. Mokhov[1]

[1] Ioffe Institute,
St. Petersburg, Russia
[2] Institute of Physics, Kazan Federal University,
Kazan, Russia

E-mail: siclab@mail.ioffe.ru

Received November 21, 2025
Revised November 21, 2025
Accepted December 27, 2025

The spin and optical properties of nitrogen-vacancy defects (NV$^-$ defects) in diamond have formed the basis for the development of opticallypumped solid-state quantum magnetometers based on this material. Significant progress has recently been achieved in the study of NV$^-$ defects in SiC, which are direct analogues of NV$^-$ defects in diamond. This paper presents the results of a study of the coherent properties of NV defects in SiC crystals with natural and reduced content of 29Si magnetic nuclei. It is shown that a decrease in the concentration of magnetic silicon isotopes can improve the coherent characteristics of NV centers. A comparative analysis of the effective transverse relaxation time (T_2^*) of NV defects in both types of matrices is performed to evaluate their suitability for application in quantum magnetometry, especially in the context of recent progress in the creation of highly stable NV defects in nanoscale SiC structures.

Keywords: Aluminum nitride, p-type doping, diffusion of Beryllium, optical absorption.

DOI: 10.61011/PSS.2026.01.63233.288-25

1. Introduction

The measurement of magnetic fields based on the quantum properties of point defects in solids is one of the rapidly developing areas of quantum sensing [1–4]. At the same time, the range of studies covers both defects in three-dimensional crystals, such as diamond and silicon carbide (SiC) [5,6], and shifts towards two-dimensional materials with a Van der Waals type of interplane bonds [7,8], revealing a wide variety of spin systems, each of which It has its own advantages and limitations for implementing quantum magnetometers based on them. The most studied system in this direction is a negatively charged nitrogen vacancy defect (NV$^-$) in diamond [3,4,9]. Due to the possibility of optical initialization and reading of the spin state $m_S = 0$ in its basic triplet state ($S = 1$), optically-detected magnetic resonance (ODMR) is implemented for the NV$^-$-center. In this case, the principle of operation is based on the registration of frequency shifts of spin resonance, which are determined by two main mechanisms: the splitting of spin sublevels of the ground state in a zero-field splitting (ZFS) with the parameter D, as well as the Zeeman interaction with an external magnetic field B. Thus, optically induced spin alignment and the presence of spin-dependent luminescence of the defect, which make it possible to register magnetic resonance using the ODMR method, are necessary conditions for the implementation of optically pumped quantum magnetometers. The fundamental sensitivity of such magnetometers is limited by the effective transverse coherence time T_2^*, which determines the inhomogeneous broadening of the spin resonance line and characterizes the decay rate of free spin precession under the influence of spin-spin interactions and static inhomogeneities of the local magnetic environment, for example, the magnetic moments of the surrounding nuclei. For an ensemble of N spins, the minimum magnetic sensitivity during measurement of τ can be expressed as

$$\eta \approx \frac{1}{g\mu_B C\sqrt{NT_2^*}},$$

where g is the gyromagnetic factor of the paramagnetic defect, μ_B is the Boron magneton, C is the contrast coefficient of the ODMR signal [10,11].

It follows from this estimate that the sensitivity requires an optimal increase in the coherence time of T_2^* in combination with high values of N paramagnetic centers, high optical reading efficiency, and scalability of the number of spin centers detected. For ensembles of NV$^-$-centers in diamond, as a result of a number of studies, optimal combinations of these key parameters have been determined [9,11–14]. So the times T_2^* are in the range of hundreds of nanoseconds ($100-300$ ns), the contrast C is about 0.3, N is in the range of $0.012-10$ ppm, which corresponds to concentrations of the order of $2\cdot10^{15}-2\cdot10^{18}$ cm^{-3} [11,13,14]. These parameters correspond to the sensitivity to the magnetic field, per unit volume of diamond of the order of $10^{-13}T^*$ (Hz $\cdot$ mm^3)$^{-1/2}$ [11,14]. To date, optical pumped quantum magnetomers based on NV$^-$-centers in diamond have found applications in condensed matter physics [2], biology and living systems [15], Earth and planetary sciences [16], in industrial magnetometry [17], and also led to the creation of a fundamentally new class of

nuclear magnetic resonance sensors that make it possible to study the properties of single nuclear spins with nanoscale resolution [18].

The successes achieved in the field of NV defects in diamond have stimulated the search for alternative solid-phase spin systems with similar or even more advantageous characteristics, but at the same time better suited for technological integration. In this context, defects in silicon carbide have attracted considerable attention from researchers, due to the fact that this material is a mature semiconductor platform with advanced technology for manufacturing devices and obtaining substrates with specified characteristics up to 6 inches in diameter [5,19–24]. This opens up broad prospects for the creation of scalable quantum sensors. In addition, defects in SiC have a number of unique properties beneficial for sensing, such as the fact that they are optically active in the near infrared range, which ensures deep penetration of radiation into biological tissues and low absorption in standard fiber-optic lines. Secondly, the spin states of many centers in SiC have different spin multiplicities and are characterized by a triplet state like divacances [25,26], or a quartet state ($S = 3/2$) in the case of negatively charged vacancies of silicon [5].

Of particular interest at the moment is the negatively charged nitrogen vacancy defect in SiC, due to the fact that it is a direct analogue of the NV^- defect in diamond. Structurally, it is formed due to a silicon vacancy in the negative charge state (V_{Si}^-) and the nitrogen atom closest to this vacancy, which replaces the carbon atom in the lattice (N_C), thereby forming a paired defect N_CV_{Si} [27,28]. Its crystal structure in the case of the hexagonal polytype 6*H* is shown in Figure 1, *a*. This polytype is characterized by the presence of three unequal positions: one hexagonal (h) and two quasi-cubic ($k1$, $k2$). Accordingly, the defect N_CV_{Si} in 6*H* can be implemented as three axial configurations — NV_{hh}, NV_{k2k1} and NV_{k1k2}, as well as three basal configurations NV_{hk1}, NV_{k1h} and NV_{k2k2}. In this paper we will focus on the example of one axial center, namely NV_{k2k1}. Particular interest to axial NV defects is attributable to their structural similarity to the NV defect in diamond [27–29], the presence of spin-dependent photoluminescence in the near infrared range with pronounced phononless lines at low temperatures (Figure 1, *b*), and the intercombination conversion channel (Figure 1, *c*), which leads to an inverse population of the spin sublevel with the projection $m_S = 0$ of the main triplet ($S = 1$) NV state$^-$.

Currently, the properties of such defects are actively studied in all SiC polytypes, in particular, their optical characteristics have been established, methods for their generation by irradiation with high-energy particles and high-temperature annealing have been developed [27,30,31], and technologies for the controlled creation of NV defects in SiC [32] nanostructures have been developed. In addition, due to spin-dependent photoluminescence, the spin resonance signal of NV defects in SiC is experimentally recorded by the ODMR method [33].

In this paper, we present the results of studies of the coherence properties of NV^- centers in isotopically modified SiC in order to demonstrate their applicability and high prospects for creating optically pumped quantum magnetometers.

2. Experimental part

Silicon carbide crystals 6*H*-^{28}SiC with a reduced content of the magnetic isotope silicon ^{29}Si were obtained by sublimation vapor deposition at high temperatures (PVT) [24] using a precursor enriched in the nonmagnetic isotope ^{28}Si. A standard plate of 6*H*-SiC with a natural isotopic composition was used as a seed substrate: ^{29}Si (4.7 %, $I = 1/2$), ^{28}Si (92.2 %, $I = 0$), ^{30}Si (3.1 %, $I = 0$), as well as carbon isotopes ^{12}C (98.9 %, $I = 0$) and ^{13}C (1.1 %, $I = 1/2$). An industrially available powder precursor with a purity level of 99.98 % in terms of the content of this isotope was used as the source of the ^{28}Si isotope. Thus, the concentrations of the isotopes ^{29}Si and ^{30}Si in the starting material were reduced by more than an order of magnitude compared with their natural content. To create NV^--defects, the grown samples were irradiated with electrons with an energy of 2 meV at a dose of $2 \cdot 10^{18}$ cm^{-2} [31], after which the samples were annealed at a temperature of 900 °C for two hours in an argon atmosphere. Electron paramagnetic resonance (EPR) experiments were performed in pulsed mode using a Bruker E680 commercial spectrometer in the frequency range of 94 GHz (W-band). Pulsed EPR spectra were recorded by measuring the integral intensity of the electron spin echo (ESE) signal as a function of the magnetic field **B** using the Hahn sequence: $\pi/2-\tau-\pi-\tau-$ESE. The duration of the $\pi/2$-pulse was 44 ns, and the delay was $\tau = 280$ ns. These studies were performed at room temperature ($T = 300$ K) and with optical excitation of NV defects in SiC by a laser with a wavelength of 980 nm. The effect of substitution of ^{29}Si isotopes with ^{28}Si isotopes was demonstrated by a comparative analysis of the dynamic and spectral characteristics of NV^- in the crystal of 6*H*-^{28}SiC and the crystal of 4*H*-SiC with a natural content of the isotope ^{29}Si, NV defects in which were created by irradiating the crystal with protons followed by high-temperature annealing [36].

3. Results and discussion

The EPR spectrum recorded on the sample of 6*H*-^{28}SiC in the electron spin echo mode in the W range at a temperature of $T = 300$ K with optical excitation by a laser $\lambda = 980$ nm is shown in Figure 2, *a*. The set of axial NV^- centers is marked with arrows indicating the splitting between the lines along the magnetic field ΔB. These observed splits between pairs of EPR spectral lines correspond to twice the amount of splitting of the spin sublevels of triplets in the Zero Field Splitting, which is

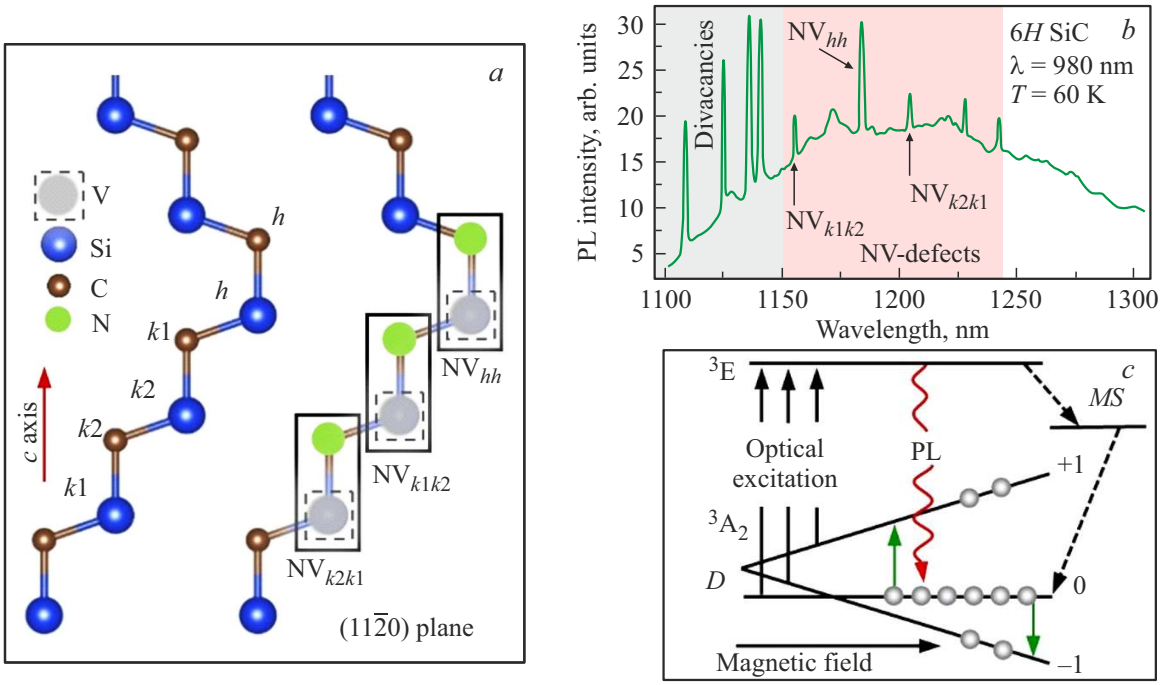

Figure 1. (a) Structure 6H-SiC in the plane 11-20. Silicon, carbon, and nitrogen atoms are shown in blue, brown, and green, respectively. The hexagonal (h) and quasi-cubic ($k1$, $k2$) unequal positions are indicated respectively. The vacancy of silicon (V) is indicated by a dotted rectangle. The axial configurations NV_{k1k2}, NV_{k2k1}, and NV_{hh} are indicated by rectangles. (b) The photoluminescence spectrum of the 6H-SiC crystal with NV defects recorded at $T = 60$ K and optical excitation of the sample with a wavelength of $\lambda = 980$ nm. The area of zero-phonon lines (ZPL) corresponding to divacancies is indicated by gray shading; the area of ZPL of NV defects is shown by light-red shading with the designation of NV defect configurations corresponding to ZPL [28,34,35]. (c) Energy structure of levels in the optical pumping cycle of spin sublevels of the NV^- defects triplet ground state. Spin-dependent recombination from the excited state (^{3}E) to the ground state ($^3A_2$) through the metastable state (MS) under optical excitation is shown by dotted arrows. The spin-dependent IR photoluminescence is denoted as PL. The separation of spin sublevels in the absence of an external magnetic field is characterized by the fine structure parameter D and is indicated accordingly. An external static magnetic field leads to the Zeeman splitting of spin sublevels into states $m_S = 0$, $m_S = +1$ and $m_S = -1$. The inverse population of the state $m_S = 0$ due to optical pumping is schematically represented by gray spheres. The green arrows indicate the allowed EPR transitions.

indicated as D in the energy diagram of the levels in Figure 1, c. Namely, $\Delta B \simeq 2D/g\mu_B$, where g is the electronic g factor $g \approx 2.00$, μ_B is the Boron magneton. Based on the measured values of ΔB , the parameters of D were calculated for various triplet states, which makes it possible to unambiguously determine the defect configuration. The values obtained are as follows: NV_{k1k2} — $D \approx 1.36$ GHz, for NV_{hh} — $D \approx 1.33$ GHz, for NV_{k2k1} — $D \approx 1.28$ GHz. These results are consistent with previously established data from studies of these defects using the EPR method [28,31]. It can also be seen from the spectra that optical excitation leads to a redistribution of the populations of the spin sublevels, namely, to the inverse population of the spin sublevel $m_S = 0$ relative to the state $m_S = -1$ in the ground state. The corresponding scheme of such optical pumping was discussed in Figure 1, c. The spectrum shows that due to spin-dependent recombination, there is preferential population of $m_S = 0$ from the excited state ^{3}E via the metastable state (MS) to the ground state. Thus, one of the necessary conditions for the implementation of optically pumped quantum magnetometers, namely, optically induced redistribution of the spin population, is well performed for NV^- defects in SiC. The lower spectrum in Figure 2, a, registered on the sample 4H-SiC, also contains signals from NV defects in this polytype. Similarly to the case of 6H-SiC, an optically induced inverse population of triplet sublevels is visible, however, the line widths in SiC with a natural content of ^{29}Si isotopes significantly exceed the line widths of NV defects in SiC with a reduced content of ^{29}Si. This observation is illustrated in Figure 2, b, c, from which it can be seen that the hyperfine structure caused by the interaction of the electron spin of NV centers with the nuclear spin of ^{14}N is well resolved in the case of NV centers in 6H-^{28}SiC, whereas in the case of 4H-SiC, the HFS is blurred due to the broadening of its components by interaction with the nuclear magnetic moments of the ^{29}Si isotope.

This situation is more clearly shown in Figure 2, c, in which the low-field components of the EPR spectra of NV centers are plotted on a centered scale of magnetic fields to the center of gravity of the EPR line. It should be noted that the values of the hyperfine interaction with

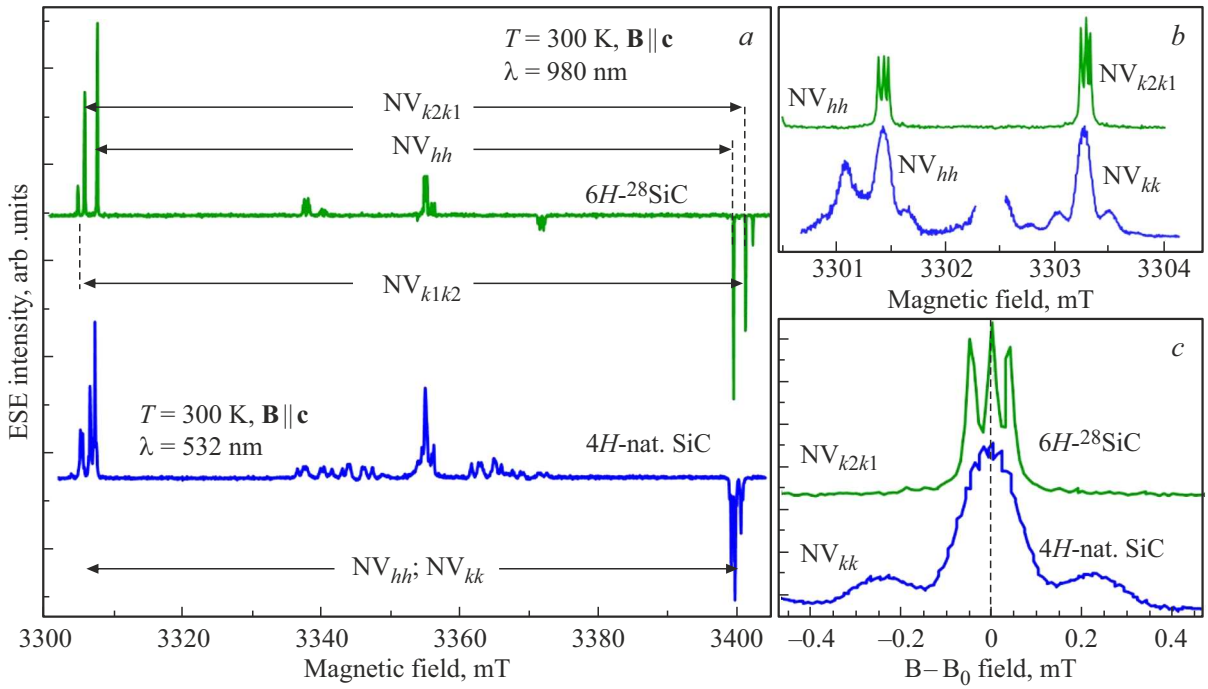

Figure 2. (*a*) The EPR spectrum of NV^- defects in 6*H*-^{28}SiC detected under the orientation of an external magnetic field **B** ∥ **c** and optical excitation $\lambda = 980$ nm. The EPR signals of the axial NV^- centers are indicated by horizontal arrows: NV_{hh}, NV_{k2k1}, NV_{k1k2}. The EPR spectrum of NV^- defects in 4*H*-SiC with a natural isotope content, recorded with field orientation **B**| ∥ **c** and optical excitation $\lambda = 532$ nm is shown below. The horizontal arrow shows the transitions from NV_{hh}, and NV_{kk} defects. (*b*) EPR transitions of NV^- centers in a low magnetic field are shown on an enlarged scale. (*c*) Comparison of the shape of EPR lines of NV_{k2k1} in 6*H*-^{28}SiC and NV_{kk} in 4*H*-SiC. In the case of 6*H*-^{28}SiC, an hyperfine structure (HFS) is visible, resulting from the interaction of the electron spin of NV centers with the nuclear spin ^{14}N ($I = 1$), in the case of 4*H*-SiC the three lines of the HFS are blurred by broadening due to interactions with the magnetic moments of ^{29}Si atoms. The spectra are plotted in coordinates $\mathbf{B} - \mathbf{B}_0$, where $\mathbf{B}_0$ corresponds to the values of the resonant magnetic fields of the center of the mass of the EPR line.

nitrogen for NV centers in both polytypes are approximately the same and amount to about 1.2 MHz. It is evident that the width of the hyperfine components for NV^- centers in 6*H*-^{28}SiC is significantly smaller than the corresponding parameters for NV centers in diamond. The broadening of the magnetic resonance line due to hyperfine interaction with surrounding nuclei is a limiting factor for the effective time of transverse spin relaxation (phase coherence), which is generally defined as $T_2^* = 1/(\gamma_e H_{1/2})$, where $H_{1/2}$ is the width of the line at half height in units of a constant magnetic field, and γ_e is the gyromagnetic ratio for an electron. Thus, it can be seen that the parameter T_2^*, which determines the sensitivity of the magnetometer, in the case of NV^- centers in 6*H*-^{28}SiC looks preferable to the similar one in the SiC crystal with a natural content of the ^{29}Si isotope. The results of direct measurements of the effective transverse relaxation time by recording the decay of free induction after a microwave $\pi/2$ pulse for NV defects in both SiC crystals are shown in Figure 3.

The analysis of the data presented in Figure 3 demonstrates significant differences in the time parameters of the transverse spin relaxation of T_2^* NV centers in the SiC matrix with a reduced content of the ^{29}Si isotope compared

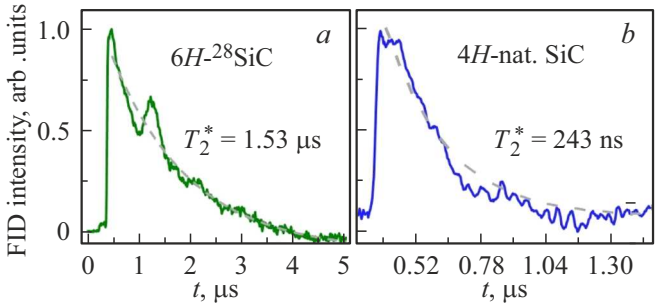

Figure 3. Transverse spin relaxation time dependences measured for NV_{k2k1} in 6*H*-^{28}SiC and NV_{kk} in 4*H*-SiC. The decay of the free induction signal is well described by a monoexponential function of the form $I(t) = A_0 \cdot e^{(-t/(T_2^*)}$ with the fitting parameter $T_2^* = 1.53\,\mu$s and $T_2^* = 243$ ns for NV_{k2k1} in 6*H*-^{28}SiC and NV_{kk} in 4*H*-SiC, respectively (dotted envelope).

with matrices with a natural isotopic composition. Thus, a change in the isotopic composition of SiC leads to a significant change in the spin coherence time, and since the sensitivity of the magnetometer is inversely proportional to the square root of this time, it can be expected that it can be increased approximately twofold.

4. Conclusion

This paper presents a comparative study of the coherent properties of NV defects in SiC crystals with a natural and reduced content of the ^{29}Si isotope. It is shown that the isotopic modification, which leads to a decrease in the concentration of magnetic nuclei, significantly increases the effective time of transverse coherence T_2^*, which, in turn, increases the sensitivity of optically pumped quantum magnetometers. As follows from the assessment of the extreme sensitivity of magnetometers discussed in the introduction, achieving high values of T_2^* while maintaining a high concentration of ODMR contrast is a key condition for the implementation of sensitive sensors. In this context, isotopically purified SiC crystals exhibit parameters comparable or superior to similar diamond-based systems, especially given the technological simplicity and high scalability of obtaining NV defects in SiC. An additional advantage is the high compatibility of silicon carbide with nanofabrication. The possibility of creating nanoscale structures based on SiC opens the way to the development of nanodisolution quantum magnetometers, which is an advanced scientific field. At the same time, manufacturing probes from SiC seems to be less laborious compared to diamond analogues, which can significantly simplify the integration of quantum sensors into applied devices similar to atomic force microscopes.

Thus, the results presented in this paper demonstrate that isotopically modified SiC crystals are a promising platform for creating quantum magnetometers that combine high sensitivity, compactness, and technological compatibility with modern micro- and nanofabrication methods.

Funding

This study was conducted under the state assignment FFUG-2024-0024 „Functional materials for microelectronics and photonics“.

Conflict of interest

The authors declare that they have no conflict of interest.

References

[1] R. Budakian, A. Finkler, A. Eichler, M. Poggio, C.L. Degen, S. Tabatabaei, I. Lee, P-C. Hammel, S.P. Eugene, T.H. Taminiau, R.L. Walsworth, P. London, A. Bleszynski Jayich, A. Ajoy, A. Pillai, J. Wrachtrup, F. Jelezko, Y. Bae, A.J. Heinrich, C.R. Ast, P. Bertet, P. Cappellaro, C. Bonato, Y. Altmann, E. Gauge. Nanotechnology, **35**, 41 (2024).

[2] F. Casola, T. van der Sar, A. Yacoby. Nat. Rev. Mater. **3**, 17088 (2018).

[3] A.K. Dmitriev, A.K. Vershovskii. Technical Physics **65**, *8*, 1301–1306 (2020)

[4] R.A. Babunts, A.A. Soltamova, D.O. Tolmachev, V.A. Soltamov, A.S. Gurin, A.N. Anisimov, V.L. Preobrazhenskii, P.G. Baranov. JETP Lett. **95**, *8*, 429–432 (2012)

[5] S.A. Tarasenko, A.V. Poshakinskiy, D. Simin, V.A. Soltamov, E.N. Mokhov, P.G. Baranov, V. Dyakonov, G.V. Astakhov. Phys. Status Solidi B **255**, 1 (2018).

[6] K.V. Likhachev, M.V. Uchaev, I.P. Veyshtort, A.V. Batueva, A.S. Gurin, R.A. Babunts, P.G. Baranov. J. Appl. Phys. **137**, 015701 (2025).

[7] S. Vaidya, X. Gao, S. Dikshit, I. Aharonovich, T.Li. Advances in Physics: X 8 (2023).

[8] A. Gottscholl, M. Diez, V. Soltamov, C. Kasper, D. Krause, A. Sperlich, M. Kianinia, C. Bradac, I. Aharonovich, V. Dyakonov. Nat. Commun. **12**, 4480 (2021).

[9] M.W. Doherty, N.B. Manson, P. Delaney, F. Jelezko, J. Wrachtrup, L. CL Hollenberg. Phys. Rep. **528**, *1*, 1–45 (2013).

[10] D. Budker, M. Romalis. Nat. Phys. **3**, 227 (2007).

[11] V.M. Acosta, E. Bauch, M.P. Ledbetter, C. Santori, K.-MC. Fu, P.E. Barclay, R.G. Beausoleil, H. Linget, J.F. Roch, F. Treussart, S. Chemerisov, W. Gawlik, D. Budker. Phys. Rev. B **80**, 115202 (2009).

[12] J.H.N. Loubser, J.A. van Wyk, Rep. Progr. Phys. **41**, 1202 (1978)

[13] J.F. Barry, J.M. Schloss, E. Bauch, M.J. Turner, C.A. Hart, L.M. Pham, R.L. Walsworth, Rev. Mod. Phys. **92**, 015004 (2020).

[14] S.V. Bolshedvorskii, S.A. Tarelkin, V.V. Soshenko, I.S. Cojocaru, O.R. Rubinas, V.N. Sorokin, V.G. Vins, A.N. Smolyaninov, S.G. Buga, A.S. Galkin, T.E. Drozdova, M.S. Kuznetsov, S.A. Nosukhin, A.V. Akimov. Phys. Status Solidi RRL, **1**, *7*, 2200415 (2023).

[15] R. Schirhagl, K. Chang, M. Loretz, C.L. Degen. Annu. Rev. Phys. Chem. **65**, 83–105 (2014). 10.1146/annurev-physchem-040513-103659

[16] D.R. Glenn, R.R. Fu, P. Kehayias, D. Le Sage, E.A. Lima, B.P. Weiss, R.L. Walsworth. Geochem. Geophys. Geosyst. **18**, 3254 (2017).

[17] A. Grosz, M.J. Haji-Sheikh, S.C. Mukhopadhyay. High Sensitivity Magnetometers (Springer, N.Y.), (2017).

[18] I. Schwartz, J. Rosskopf, S. Schmitt, B. Tratzmiller, Q. Chen, L.P. McGuinness, F. Jelezko, M.B. Plenio. Sci. Rep. **9**, 6938 (2019). https://doi.org/10.1038/s41598-019-43404-2

[19] V.A. Soltamov, B.V. Yavkin, A.N. Anisimov, H. Singh, A.P. Bundakova, G.V. Mamin, S.B. Orlinskii, E.N. Mokhov, D. Suter, P.G. Baranov. Phys. Rev. B, **103**, 195201 (2021). DOI: 10.1103/PhysRevB.103.195201

[20] P.G. Baranov, A.P. Bundakova, A.A. Soltamova, S.B. Orlinskii, I.V. Borovykh, R. Zondervan, R. Verberk, J. Schmidt. Phys. Rev. B **83**, 125203 (2011).

[21] D. Awschalom, R. Hanson, J. Wrachtrup, B.B. Zhou. Nat. Photonics, **12**, 516–527 (2018). DOI: 10.28/s411566-188-0232-1

[22] X. Chen, X. Yang, X. Xie, Y. Peng, L. Xiao, C. Shao, H. Li, X. Hu, X. Xu. Light: Science & Applications (2023). 12:28 Official journal of the CIOMP 2047-7538 https://doi.org/10.1038/s41377-022-01037-7

[23] H.I. Helava, E.N. Mokhov, O.A. Avdeev, M.G. Ramm, D.P. Litvin, A.V. Vasiliev, A.D. Roenkov, S.S. Nagalyuk, Y. Makarov. Mater. Sci. Forum **742**, 85–90 (2013).

[24] https://www.powerwaywafer.com/4h-semi-insulating-sic.html

[25] P.G. Baranov, I.V. Il'in, E.N. Mokhov, M.V. Muzafarova, S.B. Orlinskii, J. Schmidt. JETP Lett. **82**, 441 (2005).

[26] V.S. Vainer, V.A. Il'in. Sov. Phys. Solid State **23**, 2126 (1981).

[27] A. Csóré, H.J. von Bardeleben, J.L. Cantin, A. Gali. Phys. Rev. B, **96**, 085204 (2017). DOI: 10.1103/PhysRevB.96.085204
[28] Kh. Khazen, H.J. von Bardeleben, S.A. Zargaleh, J.L. Cantin,1 Mu Zhao, W. Gao, T. Biktagirov, U. Gerstmann. Phys. Rev. B, **100**, 205202 (2019).
[29] F.F. Murzakhanov, B.V. Yavkin, G.V. Mamin, S.B. Orlinskii, H.J. von Bardeleben, T. Biktagirov, U. Gerstmann, V.A. Soltamov. Phys. Rev. B, **103**, 245203 (2021). DOI: 10.1103/PhysRevB.103.245203
[30] S.I. Sato, T. Narahara, Y. Abe, Y. Hijikata, T. Umeda, T. Ohshima. J. Appl. Phys., **126**, 083105 (2019). DOI: 10.1063/1.5099327
[31] F.F. Murzakhanov, Yu.A. Uspenskaya, E.N. Mokhov, O.P. Kazarova, V.V. Kozlovsky, V.A. Soltamov. FTT **66**, *4*, 537–541 (2024) (in Russian).
[32] V.A. Norman, S. Majety, A.H. Rubin, P. Saha, N.R. Gonzalez, J. Simo, B. Palomarez, L. Li, P.B. Curro, S. Dhuey, S. Virasawmy, M. Radulaski. ACS Photonics **12**, *5*, 2604–2611 (2025).
[33] J.-F. Wang, F.-F. Yan, Q. Li, Z.-H. Liu, H. Liu, G.-P. Guo, L.-P. Guo, X. Zhou, J.-M. Cui, J. Wang, Z.-Q. Zhou, X.-Y. Xu, J.-S. Xu, C.-F. Li, G.-C. Guo. Phys. Rev. Lett. **124**, 223601 (2020).
[34] A.L. Falk, B. B. Buckley, G. Calusine, W.F. Koehl, V.V. Dobrovitski, A. Politi, C.A. Zorman, P.X.-L. Feng, D.D. Awschalom. Nat. Commun. **4**, 1819 (2013). https://doi.org/10.1038/ncomms2854
[35] Yu.E. Ermakova, I.N. Gracheva, F.F. Murzakhanov, A.N. Smirnov, I.A. Eliseev, O.P. Kazarova, G.V. Mamin, M.R. Gafurov. Pisma v ZhETF **122**, *1–2*, 116–122 (2025) (in Russian).
[36] H.J. von Bardeleben, J.L. Cantin, E. Rauls, U. Gerstmann. Phys. Rev. B **92**, 064104 (2015).

Translated by A.Akhtyamov